IOP PUBLISHING JOURNAL OF PHYSICS A: MATHEMATICAL AND THEORETICAL

J. Phys. A: Math. Theor. **43** (2010) 125102 (13pp) doi:10.1088/1751-8113/43/12/125102

Torus breakdown and noise-induced dynamics in the randomly driven Morse oscillator

Chunbiao Gan[1], **Qingyun Wang**[2] **and Matjaž Perc**[3]

[1] Institute of Applied Mechanics, School of Aeronautics and Astronautics, Zhejiang University, Hangzhou 310027, People's Republic of China
[2] School of Statistics and Mathematics, Inner Mongolia Finance and Economics College, Huhhot 010071, People's Republic of China
[3] Department of Physics, Faculty of Natural Sciences and Mathematics, University of Maribor, Koroška cesta 160, SI-2000 Maribor, Slovenia

Received 10 August 2009, in final form 19 January 2010
Published 3 March 2010
Online at stacks.iop.org/JPhysA/43/125102

Abstract
Strictly, the KAM torus no longer exists for a randomly driven Hamiltonian system. We firstly investigate the process of torus breakdown in the randomly driven Morse oscillator by transforming the original system into another one in action-angle variables and introducing the specific Poincaré map by Makarov *et al*. Though the strength of random perturbations is large, some thick closed-like curves can still appear. To characterize these noisy dynamics, the pseudo-periodic surrogate approach, along with the algorithm on the mean divergence, is applied to evaluate the correlation dimensions of the original data and their corresponding surrogates. Two kinds of noisy dynamics are picked out from the randomly driven Morse oscillator.

PACS number: 05.45.+b

1. Introduction

In Hamiltonian systems, regular motions, i.e. motions on various KAM tori, are fundamental [1, 2]. From the KAM theory, a set of invariant closed curve can survive with positive Lebesgue measure if the strength of perturbation is sufficiently small. The surviving invariant closed curves are filled with dense irrational orbits [3, 4]. In hyperbolic chaotic scattering, all the periodic orbits are unstable and there are no KAM tori in the phase space. However, nonhyperbolic deterministic systems are endowed with mixed phase space partitioned into stable and unstable regions, and KAM tori coexist with other chaotic sets [5, 6], which typically results in algebraic decay in the survival probability of a particle in the scattering region due to the stickness effect of KAM tori [2].

A physically important issue in the study of nonlinear dynamics is to understand how robust a phenomenon is against perturbations or deviations between the underlying

mathematical model and physical reality. As studied in [7], weak dissipation can have a metamorphic consequence on nonhyperbolic chaotic scattering in the sense that the physically important particle-decay law is altered, no matter how small the amount of dissipation. If a system is subjected to a random force, the problem of finding an exact solution of the equations of motion is often replaced by the problem of finding the respective probability density function in phase space. In [8], Dykman *et al* discussed activated escape from a metastable state of a system driven by a time-periodic force, and a closed-form explicit expression for the escape rate of an overdamped Brownian particle was presented and shown to be in quantitative agreement with simulations. In addition, they also described experiments on a Brownian particle optically trapped in a double-well potential, and showed that a suitable periodic modulation of the optical intensity could break the spatio-temporal symmetry of an otherwise spatially symmetric system. In [9], Makarov *et al* investigated the phenomena of torus breakdown in the Morse oscillator driven by a band-limited Gaussian white noise, and discussed the domains of finite-time stability in phase space by introducing an excellent specific Poincaré map. It was shown that the lifetime of stable domains significantly exceeded the correlation time of the external force.

In past decades, randomly perturbed or noise-induced dynamics were discussed by the statistical method and averaging principle [10], the stochastic sensitivity function [11], the stochastic Melnikov method [12–14], the random perturbation of Poincaré map [15], etc, and several quantitive methods are combined to identify the noisy dynamics in [16, 17]. In this study, the randomly driven Morse oscillator is further illustrated to explore the phenomenon of torus breakdown and identify noisy dynamics. This paper is organized as follows. In section 2, the Morse oscillator driven by the bounded noise is firstly transformed into another form in action-angle variables, and a specific Poincaré map is then set up to investigate the phenomenon of torus breakdown. Section 3 firstly introduces some relevant numerical algorithms, such as the leading Lyapunov exponent for small data sets, the pseudo-periodic surrogate (PPS) method, etc, to identify noisy dynamics. We then present some numerical tests on the noisy quasi-periodic and noise-induced chaotic time series by the forth-mentioned algorithms. In the final section, we summarize and discuss results of this work.

2. Torus breakdown due to random perturbations

The vibrational motion of diatomic molecules can be described by the Morse oscillator, and it is frequently used in theoretical chemistry to describe the photodissociation of molecules [18]. In [9], the authors presented a specific Poincaré map for this randomly driven oscillator based on the condition of finite-time invariance and the fact that the respective random function has a certain value at any given moment of time.

Here, the Morse oscillator is assumed to be perturbed by a multiplicative bounded noise and written as

$$\begin{cases} \dot{x} = y \\ \dot{y} = \mathrm{e}^{-2x} - \mathrm{e}^{-x} + \varepsilon\, \mathrm{e}^{-x}\xi(t) \end{cases} \tag{1}$$

where ε is a small nonnegative parameter, and $\xi(t)$ is the bounded noise [19], i.e.

$$\xi(t) = \cos[\Omega t + \sigma B(t) + \gamma] \tag{2}$$

where Ω and σ are constants, $B(t)$ is a unit Wiener process and γ is a random variable uniformly distributed in the interval $[0, 2\pi)$. The two-sided spectral density of $\xi(t)$ is given by

$$S_\xi(\omega) = \frac{1}{2\pi}\left[\frac{\sigma^2}{4(\omega-\Omega)^2+\sigma^4} + \frac{\sigma^2}{4(\omega+\Omega)^2+\sigma^4}\right]. \tag{3}$$

The shape of the spectral density is determined by the Ω and σ values. In general, it has two symmetrical peaks, symmetrically located in the positive and negative frequency domains; their bandwidth depends on σ, and their locations depend on Ω and, to a less degree, and also on σ. When $\Omega/\sigma^2 \gg 1$, $\xi(t)$ becomes a narrow-band random process, while in the limit as σ approaches infinity, the random process becomes a 'white noise' of constant spectral density [19].

From [20], each physical realization of $\xi(t)$ can be approximated by

$$\eta(t) \approx \sum_{k=1}^{N} A\cos(\omega_k t + \psi_k), \qquad N \to \infty, \tag{4}$$

where $A = \sqrt{2S_\xi \Delta\omega}$, $\{\omega_k | k = 1, 2, \ldots, N\}$ are independent and nonnegative random variables over the interval $[\omega_l, \omega_r]$, $\Delta\omega$ $(=(\omega_r - \omega_l)/N)$ is a frequency increment, $\{\psi_k | k = 1, 2, \ldots, N\}$ are identically uniformly distributed over the interval $[0, 2\pi)$ and N is a fixed positive integer. For crucial aspects on this approximate description, e.g. the minimal number N in equation (4), see [20]. For a large positive integer N (see section 3), the physical realization generated by equation (4) is almost ergodic, and numerical results show that the influence of this large integer can be neglected. Since the duration of time is not concerned with the sum in equation (4), a specific Poincaré map can then be set up as in [9].

When $\varepsilon = 0$ in system (1), $(\infty, 0)$ is a hyperbolic fixed point connected to itself by a homoclinic orbit. By introducing the McGehee transformation $x = -2\log u$, $y = v$, and reparametrizing time as $\mathrm{d}s/\mathrm{d}t = -u/2$, we can find that (0,0) is the hyperbolic fixed point connected to itself by a homoclinic orbit. The Hamiltonian for system (1) is given by

$$H = H_0 + \varepsilon H_1(t) = \tfrac{1}{2}[y^2 + (\mathrm{e}^{-x} - 1)^2] + \varepsilon\,\mathrm{e}^{-x}\xi(t). \tag{5}$$

Prior to the construction of the specific Poincaré map, the action $I(=I(x, y))$ and angle θ $(=\theta(x, y))$ variables are introduced by the following formulas [21]:

$$I = \frac{1}{2\pi}\oint y\,\mathrm{d}x, \qquad \theta = \frac{\partial}{\partial I}\int_{x'}^{x} y\,\mathrm{d}x \tag{6}$$

where x' is a coordinate of one of the turning points, and y can be found from a constant Hamiltonian $H(x, y) = \text{const}$. When $\varepsilon = 0$, the solutions of system (1) can be expressed as

$$x_0(I, \theta) = \ln\frac{1 - \sqrt{1 - \Gamma^2}\cos\theta}{\Gamma^2}, \qquad y_0(I, \theta) = \frac{\Gamma\sqrt{1 - \Gamma^2}\sin\theta}{1 - \sqrt{1 - \Gamma^2}\cos\theta} \tag{7}$$

in terms of the action-angle variables, where $\Gamma \equiv \Gamma(I) = 1 - I$.

From equation (7), we can obtain the inverse relationship $(I, \theta) = (I(x_0, y_0), \theta(x_0, y_0))$, and the Hamiltonian given by equation (5) is then rewritten as

$$H = I - \frac{I^2}{2} + \varepsilon\frac{(1 - I)^2}{1 - \sqrt{1 - (1 - I)^2}\cos\theta}\xi(t). \tag{8}$$

System (1) is now transformed into the following one:

$$\begin{cases} \dfrac{\mathrm{d}I}{\mathrm{d}t} = -\dfrac{\partial H}{\partial\theta} = \varepsilon\Gamma^2\dfrac{\sqrt{1 - \Gamma^2}\sin\theta}{[1 - \sqrt{1 - \Gamma^2}\cos\theta]^2}\xi(t) \\ \dfrac{\mathrm{d}\theta}{\mathrm{d}t} = \dfrac{\partial H}{\partial I} = \bar{\omega} + \varepsilon\left\{-2\Gamma[1 - \sqrt{1 - \Gamma^2}\cos\theta] - \dfrac{\Gamma^3}{\sqrt{1 - \Gamma^2}}\cos\theta\right\}\dfrac{\xi(t)}{[1 - \sqrt{1 - \Gamma^2}\cos\theta]^2} \end{cases} \tag{9}$$

where $\bar{\omega}$ is the circular frequency of the unperturbed motion of system (1) and $\Gamma = 1 - I$.

For a periodically driven deterministic system, the existence of compact sets issues immediately from the KAM theory. However, the KAM theory cannot be directly applied

to Hamiltonian systems under random perturbations. Although each individual realization of a random process can be treated as a deterministic function (see equation (4)), the resonant values between the unperturbed and perturbed motions are densely distributed in phase space, and there is no non-destroyed invariant curve or KAM torus. In view of the stability theory, all motions of a random system are unstable in the limit $t \to \infty$, which makes a deterministic description of long-term dynamics senseless.

According to the time-limited invariability of a randomly perturbed dynamical system, it holds that any motion initiating from some set in a phase space returns to the set after a finite time without mixing. Thus, within this time interval any such ensemble of trajectories is stable according to Lyapunov [9]. So, we can study the complicated dynamics by an individual physical realization of $\xi(t)$ within some finite time interval, say $[0, T_0]$, and repetitively investigate the results from the periodical signals consisting of identical pieces of $\eta(t)$ with the same duration T_0, i.e.

$$\bar{\eta}(t + nT_0) \equiv \eta(t), \qquad t \in [0, T_0], \tag{10}$$

where n is an integer. From definition (10), the randomly perturbed dynamical system (1) is replaced by a periodically driven one, and we can observe the resonant effect of each physical realization on the unperturbed motions with different periods by choosing different T_0.

A specific Poincaré map is now constructed by the following basic rule: the values of the system's parameters, calculated at the ith step of mapping, become the initial conditions for the next step. It is defined as

$$\begin{aligned} P_\varepsilon : \Sigma^{\phi_0} &\to \Sigma^{\phi_0} \\ (I_\varepsilon(0), \theta_\varepsilon(0)) &\to (I_\varepsilon(T_0), \theta_\varepsilon(T_0)) \end{aligned} \tag{11}$$

where $\Sigma^{\phi_0} = \{(I, \theta, \phi) | \phi = \phi_0\}$ is a global cross-section. The nth iteration of the above map is given by

$$\begin{aligned} P_\varepsilon^n : \Sigma^{\phi_0} &\to \Sigma^{\phi_0} \\ (I_\varepsilon(0), \theta_\varepsilon(0)) &\to (I_\varepsilon(nT_0), \theta_\varepsilon(nT_0)). \end{aligned} \tag{12}$$

From equation (9), various values of T_0 in equation (10) may be chosen to observe different effects on tori by this specific Poincaré map (11) or (12). For the different initial action I_0, ω_0 can be calculated from the relationship

$$\omega = \frac{T(H)}{2\pi} = \frac{\partial H}{\partial I} = 1 - I, \tag{13}$$

while the initial angle θ_0 can be fixed, say $\pi/4$ or other.

Each physical realization is generated by equation (4). In this study, we set $\Omega = 1$, $\omega_l = 0.002\pi, \omega_r = 2\pi, N = 20\,000$, unless otherwise indicated. Each orbit of equation (9) is integrated over 2000 mapping periods with period T_0 by the well-known fourth-order Runge–Kutta method. For the different initial action I_0 and the fixed initial angle $\theta_0 = \pi/4$, we integrate equation (9) and record the values of the angles I and θ every sampling period T_0, and the quantities

$$I_x = I \cos\theta / I_s, \qquad I_y = I \sin\theta / I_s \tag{14}$$

can then be drawn in a figure to observe the phenomenon of torus breakdown when the system is randomly perturbed, where I_s is the most accessible action corresponding to the separatrix $H = 0.5$ and is equal to 1. Since the topology of map (11) is similar for all physical realizations of $\xi(t)$ as shown in [9], we only represent a typical set of maps from an individual realization in figures 1 and 2 with different T_0 to observe the resonant effects of the bounded noise on the system's various motions. Though the system is driven by the bounded noise, some thick

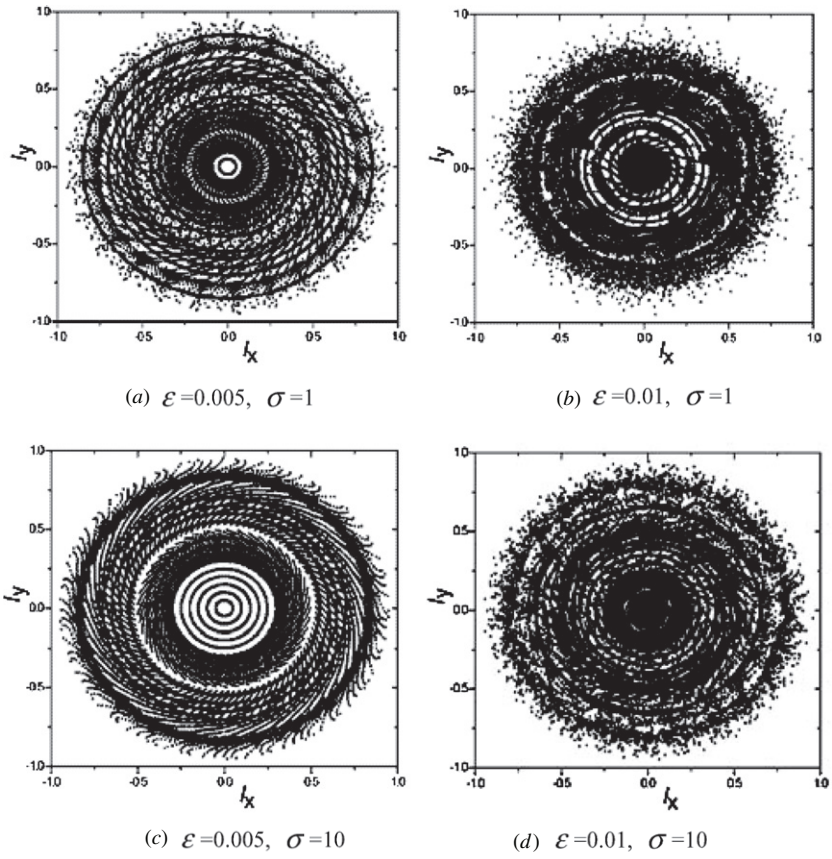

Figure 1. Torus breakdown in system (9) under random perturbation, where $T_0 = 10$.

closed-like curves can be observed clearly in each case (figures 1(*a*), (*c*) and 2(*a*), (*c*)), even for larger ε (figures 1(*b*), (*d*) and 2(*b*), (*d*)). Moreover, for different T_0 and σ, the topologies of map (11) are apparently distinguishable, which means that the effects of noise with different spectral width are different for various motions.

In [22], Arnold considered a time-dependent Hamiltonian system with two degrees of freedom, and proved that the system had an orbit which connected two different regions. In figures 1 and 2, we also observe such diffusive behaviors in the Morse system. However, since the perturbation in our case is a random force, theoretical analysis is difficult to perform at the present time, and thus there is considerable work to be done to investigate this more precisely.

3. Characterization of noise-induced dynamics

Without noisy perturbation, the dynamics of the Morse oscillator can be identified easily from the traditional dynamical theory. However, an irregular time series cannot be simply said to be chaotic when the system is randomly driven. If the strength of random perturbation is very large, then the so-called random-dominant responses will appear [16, 23]. To identify the noisy dynamics of system (1), we first introduce several numerical algorithms.

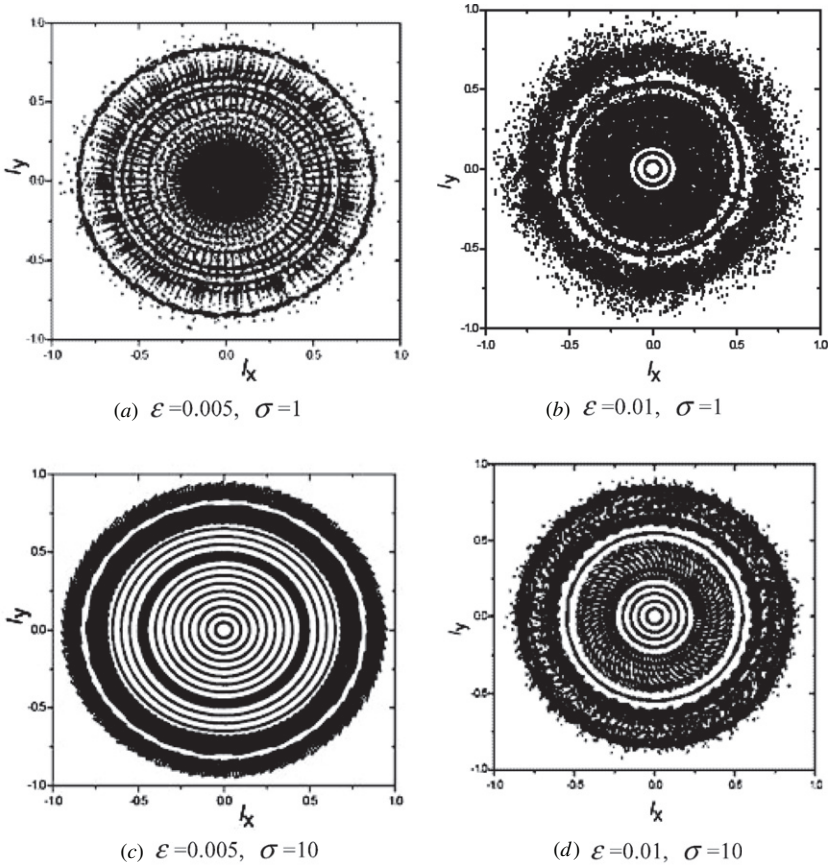

(*a*) ε =0.005, σ =1 (*b*) ε =0.01, σ =1

(*c*) ε =0.005, σ =10 (*d*) ε =0.01, σ =10

Figure 2. Torus breakdown in system (9) under random perturbation, where $T_0 = 50$.

The sensitive dependence of response on initial conditions can be quantified by the Lyapunov exponent, which characterizes the average exponential rate of divergence or convergence of nearby orbits in phase space of a system and quantifies the strength of chaos. As pointed out by Kantz and Schreiber [24], the algorithm by Wolf *et al* [25] is not very robust for random dynamics. In spite of Wolf's algorithm only using a delay reconstruction of phase space, there is another class of algorithms which also involves the approximation of the underlying deterministic dynamics. Here, Rosenstein's approach [26] is employed to compute the leading Lyapunov exponent to identify noisy dynamics. Though the output data are affected by noise, the influence from noise can be minimized by employing averaging statistics from this approach.

The first step of Rosenstein's method involves reconstructing the attractor dynamics from a single time series. The reconstructed trajectory, $\boldsymbol{X}$, is expressed as a matrix where each row is a phase-space vector, i.e. $\boldsymbol{X} = (\boldsymbol{X}_1, \boldsymbol{X}_2, \ldots, \boldsymbol{X}_M)^{\mathrm{T}}$. For a K-point time series, say $\{x_1, \ldots, x_K\}$, each $\boldsymbol{X}_i$ is given by $\boldsymbol{X}_i = (x_i, x_{i+J}, \ldots, x_{i+(m-1)J})$, where J is the lag or reconstruction delay and m is the embedding dimension. Thus, $\boldsymbol{X}$ is an $M \times m$ matrix, and the constants m, M, J and K are related as $M = K - (m-1)J$.

The basic algorithm for the computation of the response's leading Lyapunov exponent is listed as follows [26]:

(i) Solve system (1) by using the fourth-order Runge–Kutta method and the triangle series approximation (4), and record the time series $x(t)$ versus t.

(ii) Estimate the time lag and mean period of the sample time series from step (i) by using the FFT, e.g. using the median frequency of the magnitude spectrum.

(iii) Reconstruct attractor dynamics using the method of delays. The embedding dimension is usually estimated in accordance with Taken's theorem [27], i.e. $m > 2l$, where l is the number of degrees of freedom of the system. A method used to choose the lag via the correlation sum was addressed by Liebert and Schuster [28].

(iv) Find nearest neighbors and constrain temporal separation. The nearest neighbor $\mathbf{X}_{j'}$ is found by searching for the point that minimizes the distance to the particular reference point $\mathbf{X}_j$, i.e. $d_j(0) = \min_{\mathbf{X}_{j'}} \|\mathbf{X}_j - \mathbf{X}_{j'}\|$, where $d_j(0)$ is the initial distance from the jth point to its nearest neighbor, and $\|\cdot\|$ denotes the Euclidean norm. Here, an additional constraint is required, i.e. $|j - j'| >$ mean period.

(v) The leading Lyapunov exponent is estimated by

$$\lambda_1(i) = \frac{1}{i\,\Delta t}\frac{1}{(M-i)}\sum_{j=1}^{M-i}\ln\frac{d_j(i)}{d_j(0)} \tag{15}$$

where Δt is the sampling period of the time series, and $d_j(i)$ is the distance between the jth pair of the nearest neighbors after i discrete time steps, i.e. $i\,\Delta t$ seconds.

(vi) The final result for the leading Lyapunov exponent is calculated using a least-squares fit to the average line defined by $y(i) = \langle \ln(d_j(i)\rangle/\Delta t$, where $\langle\cdot\rangle$ denotes the average of all values of j. As pointed out by Rosenstein [26], the process of averaging is the key to calculate accurate values of λ_1 by using small and noisy data sets.

In [29, 30], the method of surrogate data was used by Small *et al* to test pseudo-periodic time series data and detect determinism in time series with dynamical noise contamination. This method can provide a rigorous way to apply statistical hypothesis testing to experimental time series. By the pseudo-periodic surrogate (PPS) algorithm, chaotic and noisy periodic time series were distinguished from the experimental data for the Rösslersystem and human EGG [29].

The algorithm by Theiler *et al* [31] tests only for independent noise, linear noise or statically filtered linear noise, while the PPS algorithm presented by Small *et al* [29, 30] can generate surrogates that preserve coarse deterministic features (such as periodic trends) but destroy fine structures (such as deterministic chaos). The PPS method can be applied to differentiate between chaos with dynamic noise and a noisy periodic orbit, and the basic algorithm for the PPS method presented in [29, 30] is performed according to the following steps:

(i) Reconstruct the attractor dynamics from an individual time series as described in the simulation process for the leading exponent and record the reconstructed attractor as $\mathbf{A} = \{\boldsymbol{X}_k \mid k = 1,2,\ldots,K-(m-1)J\}$, in which $\boldsymbol{X}_k = [x_k, x_{k+J}, \ldots, x_{k+(m-1)J}]$.

(ii) Choose an initial condition $S_1 \in \mathbf{A}$ at random and let $i = 1$.

(iii) Choose a near neighbor $Z_j \in \mathbf{A}$ of S_i according to the probability distribution $\mathrm{Prob}(Z_j = Z_k) \propto \exp\{(-\|Z_k - S_i\|)/\rho\}$, where the parameter ρ is called the noise radius.

(iv) Let $S_{i+1} = Z_{j+1}$ be the successor to S_i and make increment i. If $i < K$, go to step (iii).

(v) The surrogate time series is recorded as $\{(S_k)_1\} \equiv \{(S_1)_1, (S_2)_1, (S_3)_1, \ldots, (S_N)_1\}$, i.e. the scalar first components of $\{S_k\}_k$.

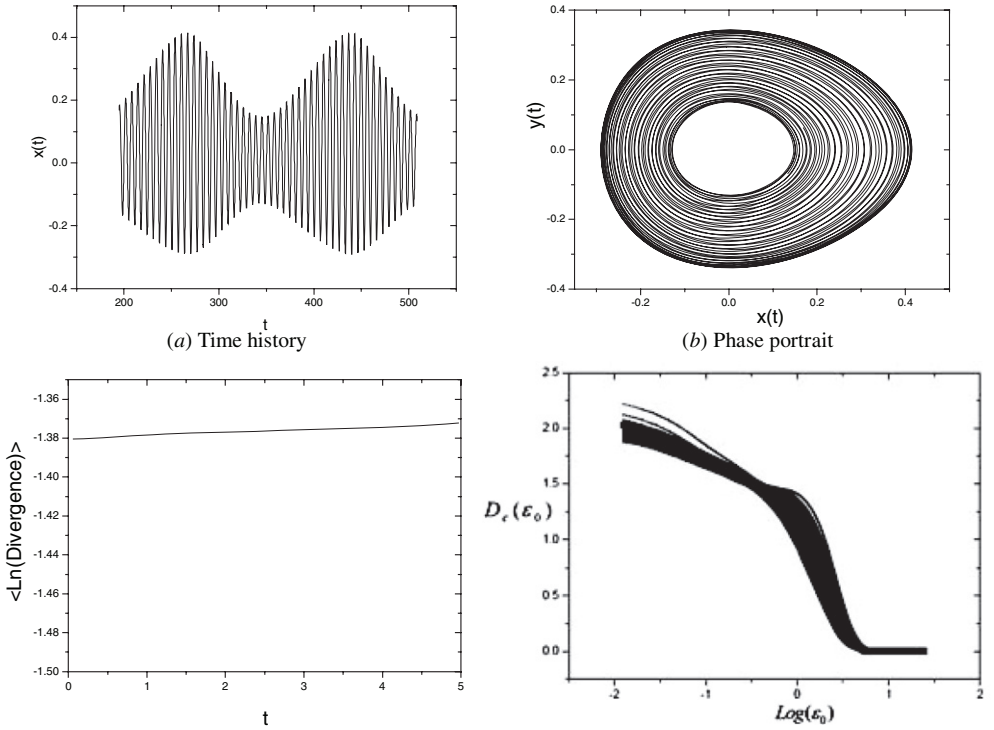

(*a*) Time history (*b*) Phase portrait

(*c*) Mean divergence (*d*) Correlation dimension

Figure 3. Noisy quasi-periodic response. The top panel shows the original data from system (1) for (*a*) time history and (*b*) phase portrait, where $\varepsilon = 0.01, \sigma = 1$. Also shown in (*c*) is the mean divergence with the embedding dimension $m = 5$ and reconstruction delay $J = 31$. Comparisons of the correlation dimensions for the original time series and surrogate data are presented in (*d*), where $\rho = 0.0001$ is the thick real line and the thin scatter lines represent the results from the original and the surrogate data, respectively. In this noisy quasi-periodic case, there is no distinction between the original data and surrogates.

In the above algorithm, the noise radius ρ can be selected such that the expected number of sequences of length 2 or more that are identical for data and surrogates is maximized [29]. This selection criterion of noise radius can provide a balance between (a) too much randomization (few identical sequences of length; and (b) too little (data and surrogate near identical).

In figures 3–6, we use the same physical realization as in figures 1 and 2 to solve the original system (1) with various initial conditions under random perturbation with different strength and spectral width. The initial condition $(x(0), y(0))$ is chosen according to the results shown in figures 1 and 2, and relationship (7) is also used, where $\theta = \pi/4$ is fixed. Two initial points of (I, θ), lying on or far away from some thick closed-like curve in figures 1 and 2, are chosen as $(0.1, \pi/4)$ and $(0.53, \pi/4)$, and correspondingly, two initial points of (x, y) are $(-0.16, 0.39)$ and $(0.53, 0.78)$ from equation (7). The sample responses evolving from the first initial value $(-0.16, 0.39)$ are shown in figures 3 and 4 with different spectral width for the random perturbation, while the sample responses evolving from the second one are presented in figures 5 and 6.

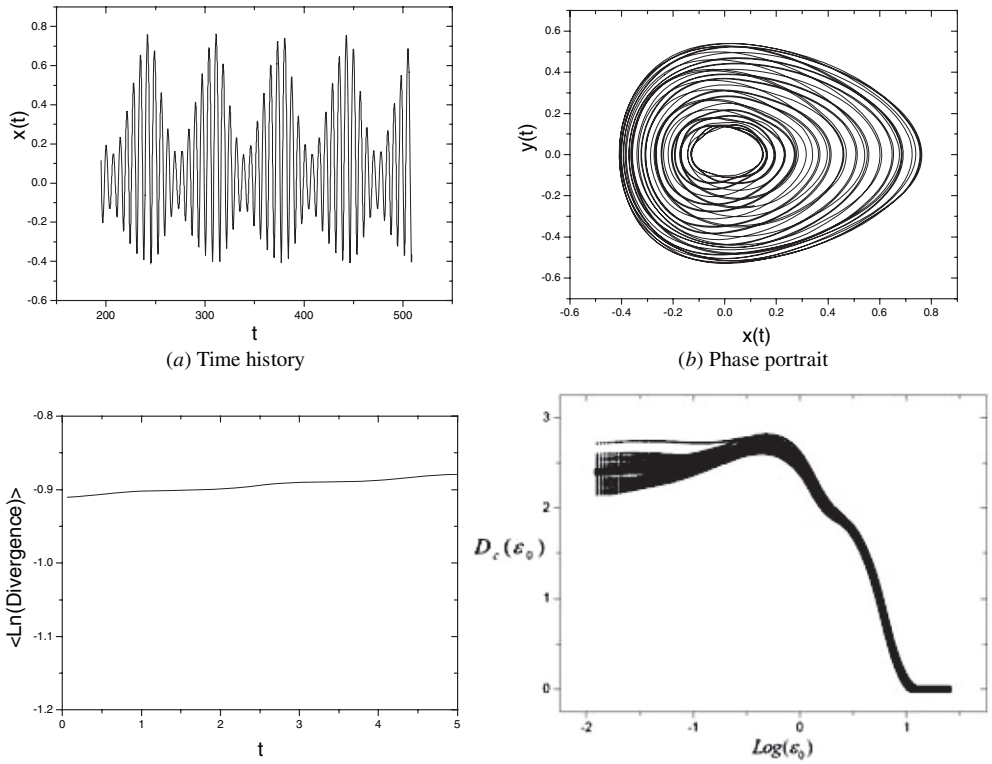

(*a*) Time history (*b*) Phase portrait

(*c*) Mean divergence (*d*) Correlation dimension

Figure 4. Noisy quasi-periodic response. The top panel shows the original data from system (1) for (*a*) time history and (*b*) phase portrait, where $\varepsilon = 0.01$, $\sigma = 10$. Also shown in (*c*) is the mean divergence with the embedding dimension $m = 5$ and reconstruction delay $J = 31$. Comparisons of the correlation dimensions for the original time series and surrogate data are presented in (*d*), where $\rho = 0.0001$ is the thick real line and the thin scatter lines represent the results from the original and the surrogate data, respectively. In this noisy quasi-periodic case, there is also no distinction between the original data and surrogates.

The parameters 't', '$x(t)$' and '$y(t)$' in figures 3–6 mean the dynamical evolving time in seconds, the displacement in meters and the velocity in meters per second, respectively. Here, the leading Lyapunov exponent of each sample response can be evaluated by the least-squares fit from the mean divergence $\langle \ln(\text{Divergence}) \rangle$ versus t curve in figures 3–6(*c*). An obvious linear slope means that the response is a chaotic one. In addition, it deserves to notify that the values of the leading Lyapunov exponents, i.e. the slopes of the obvious linear regions in the first segments of mean divergence curves, are not accurately calculated; our main goal in the current work is just to show non-chaotic and chaotic responses in the randomly driven system.

For the quasi-periodic signals contaminated with the bounded noise (figures 3 and 4(*a*), (*b*)), the original data and surrogates are indistinguishable, where the correlation dimensions are estimated according to the algorithm by Judd [32] for each original time series and 50 PPS data sets. The algorithm described in [32] estimates the correlation dimension d_c as a function of the viewing scale ε_0, so d_c for each time series is not a single number, but a curve. In these cases, the null hypothesis of a quasi-periodic orbit with uncorrelated noise

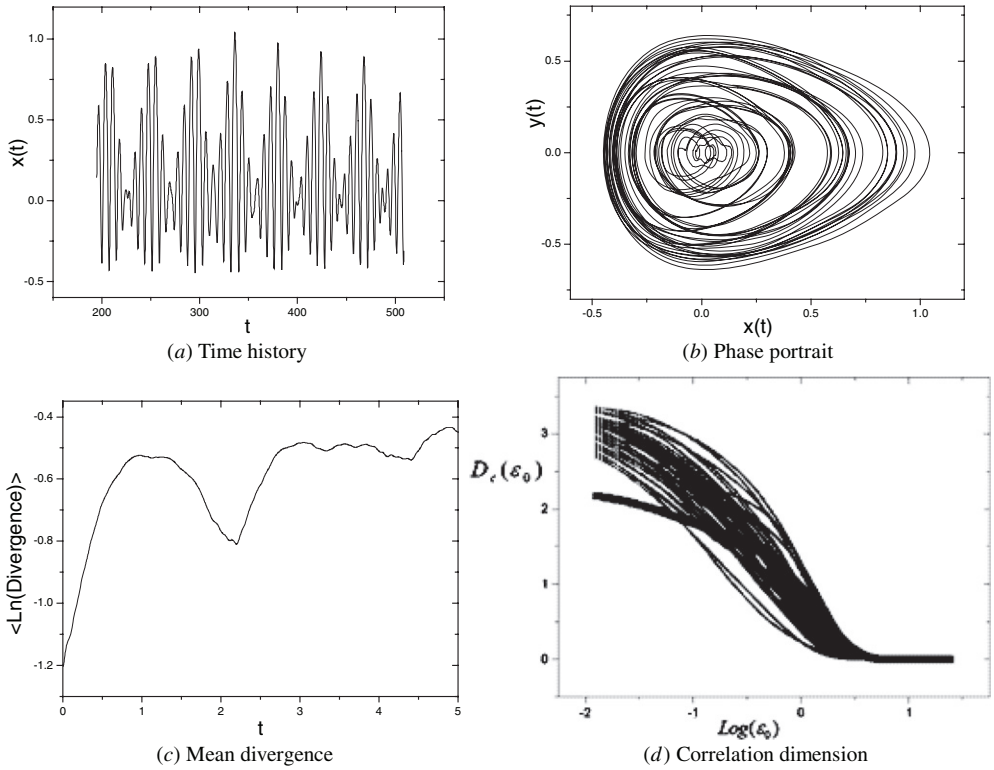

(*a*) Time history (*b*) Phase portrait

(*c*) Mean divergence (*d*) Correlation dimension

Figure 5. Noise-induced chaotic response. The top panel shows the original data from system (1) for (*a*) time history and (*b*) phase portrait, where $\varepsilon = 0.01, \sigma = 1$. Also shown in (*c*) is the mean divergence with the embedding dimension $m = 5$ and reconstruction delay $J = 31$. Comparisons of the correlation dimensions for the original time series and surrogate data are presented in (*d*), where $\rho = 0.0005$ is the thick real line and the thin scatter lines represent the results from the original and the surrogate data, respectively. In this noise-induced chaotic case, the data and surrogates are clearly distinguishable.

cannot be rejected, see figures 3 and 4(*d*). This means that quasi-periodic nature dominates the dynamical response though it is contaminated with the dynamical noise. These results are consistent with the thick closed-like curves in figures 1 and 2 and what the leading Lyapunov exponents predicted (see figures 3 and 4(*c*)), from which we can observe that the slopes of the curves are almost flat and the leading Lyapunov exponent is nearly zero.

For the noisy time series shown in figures 5 and 6, the original signals and their corresponding surrogates are clearly distinct when the viewing scale ε_0 tends to zero, and in these cases the null hypothesis of a quasi-periodic orbit with correlated noise should be rejected. From figures 5 and 6(*c*), apparent finite inclines appear in the first segments of the mean divergence curves, which means that the leading Lyapunov exponents are positive and finite, and chaotic nature dominates both the noisy time series. Since both the chaotic orbits arise from the random perturbation, we call them the noise-induced chaotic responses.

From figures 3 and 4, the noisy quasi-periodic time series can be easily picked out from other noise-contaminated dynamics of the system. However, for the noise-induced chaotic ones shown in figures 5 and 6, other measures, such as the time history and the leading Lyapunov exponent, etc, should be complemented for a proper description of the data's dynamical nature.

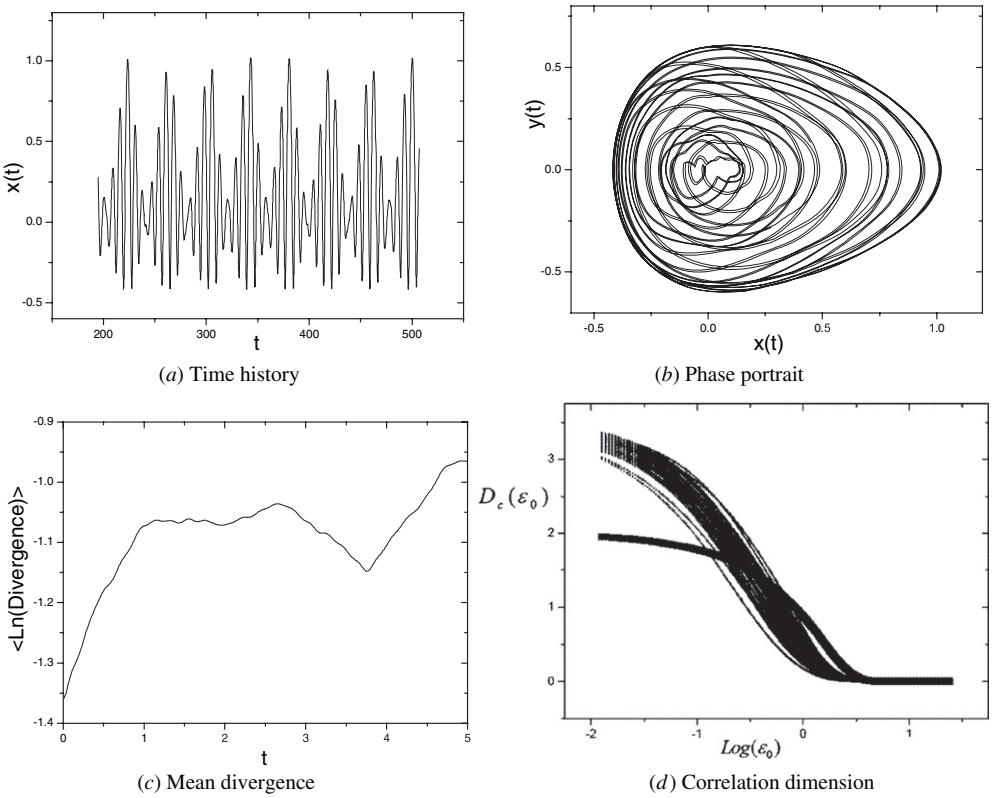

(*a*) Time history (*b*) Phase portrait

(*c*) Mean divergence (*d*) Correlation dimension

Figure 6. Noise-induced chaotic response. The top panel shows the original data from system (1) for (*a*) time history and (*b*) phase portrait, where $\varepsilon = 0.01$, $\sigma = 10$. Also shown in (*c*) is the mean divergence with the embedding dimension $m = 5$ and reconstruction delay $J = 31$. Comparisons of the correlation dimensions for the original time series and surrogate data are presented in (*d*), where $\rho = 0.0005$ is the thick real line and the thin scatter lines represent the results from the original and the surrogate data, respectively. In this noise-induced chaotic case, the data and surrogates are also clearly distinguishable.

For stronger random perturbation, the so-called random-dominant dynamics [16, 23] can arise in the system, and are not discussed here.

4. Summary and discussion

A torus in a conservative Hamiltonian system can survive under deterministic perturbation from the KAM theory or be broken down. Hyperbolic dynamics in Hamiltonian systems are typically structural stable while nonhyperbolic dynamics are not. From previous studies on random dynamics, the effect of weak random perturbation on a system's hyperbolic stable trajectory is trivial. Besides, when a random perturbation is imposed on a conservative Hamiltonian system, all responses seem irregular, especially for nonhyperbolic dynamics and stronger perturbation. In this case, we cannot simply recognize an arbitrary irregular motion as a chaotic one.

Here, the randomly driven Morse oscillator is employed as an illustrating example. For other conservative Hamiltonian systems, similar analysis can be performed. From previous

heuristic results, a specific Poincaré map is developed for the system in the form of action-angle variables and the sampling period for this map is discussed in section 2, where each physical realization of the given bounded noise process is approximated by the triangle series method. For this specific Poincaré map, various sampling periods can be chosen as required to observe the resonant effects of noises on the unperturbed motions. Here, we choose two sampling periods and change the spectral width of the bounded noise process to observe the resonant effects of the bounded noise process on the system's various motions and the phenomena of torus breakdown. It is shown that many thick closed-like curves still survive under weak random perturbation, while most original invariant tori will be broken down for stronger random perturbation. For various sampling periods, the topologies of the Poincaré map are apparently different.

Based on the instructive analysis in section 2, several quantitive algorithms are developed to identify the noisy dynamics in this system. Thick closed-like curves mean that the sample responses randomly walk within a narrow band of the original quasi-periodic trajectories. The corresponding responses are called the noisy quasi-periodic ones, which are validated by the leading Lyapunov exponents and the PPS method. However, there is no closed-like curve for the noise-induced chaotic response. Since the deterministic chaotic scattering is nonhyperbolic for the Morse oscillator, the point sets in Poincaré's global cross-section seem to be different for various chaotic responses, which is not the same as in the hyperbolic case. When this kind of noisy dynamics occurs, the PPS algorithm and the leading Lyapunov exponent play pivotal roles in its identification.

If the random perturbation becomes very strong, then there will appear the so-called random-dominant responses in the system. Our future studies will be focused on different resonant effects of random perturbation on various periodic or quasi-periodic motions, by choosing different sampling periods and increasing the strength of random perturbation, to explore more complex noisy dynamics.

Acknowledgments

The authors acknowledge the supports from the National Natural Science Foundation of China under grant nos 10672140, 10972001, 10702023 and 10832006. Matjaž Perc individually acknowledges support from the Slovenian Research Agency (grant no Z1-2032-2547).

References

[1] Moser J 1973 *Stable and Random Motions in Dynamical Systems* (Princeton, NJ: Princeton University Press)
[2] Lai Y C, Ding M, Grebogi C and Blumel R 1992 Algebraic decay and fluctuations of the decay exponent in Hamiltonian system *Phys. Rev.* A **46** 4661–9
[3] Guckenheimer J and Holmes P J 1981 *Nonlinear Oscillations, Dynamical Systems, and Bifurcations of Vector Fields* (New York: Springer)
[4] Wiggins S 1990 *Introduction to Applied Nonlinear Dynamical Systems and Chaos* (New York: Springer)
[5] Lau Y T, Finn J M and Ott E 1991 Fractal dimension in nonhyperbolic chaotic scattering *Phys. Rev. Lett.* **66** 978–81
[6] Lai Y C, Blumel R, Ott E and Grebogi C 1992 Quantum manifestations of chaotic scattering *Phys. Rev. Lett.* **68** 3491–4
[7] Motter A E and Lai Y C 2001 Dissipative chaotic scattering *Phys. Rev.* E **65** 015205 (1–4)
[8] Dykman M I, Golding B, McCann L I, Smelyanskiy V N, Luchinsky D G, Mannella R and McClintock P V E 2001 Activated escape of periodically driven systems *Chaos* **11** 587–94
[9] Makarov D and Uleysky M 2006 Specific Poincaré map for a randomly-perturbed nonlinear oscillator *J. Phys. A: Math. Gen.* **39** 489–97
[10] Szopa J 1984 Sensitivity of stochastic systems to initial conditions *J. Sound Vib.* **97** 645–9

[11] Freidlin M I and Wentzel A D 1984 *Random Perturbations in Dynamical Systems* (New York: Springer)
[12] Frey M and Simiu E 1993 Noise-induced chaos and phase space flux *Physica* D **63** 321–40
[13] Simiu E and Frey M 1996 Melnikov processes and noise-induced exits from a well *J. Eng. Mech.* **122** 263–70
[14] Lin H and Yim S C S 1996 Analysis of a nonlinear system exhibiting chaotic, noisy chaotic, and random behaviors *J. Appl. Mech. ASME* **63** 509–16
[15] Kapitaniak T 1990 *Chaos in Systems with Noise* (Singapore: World Scientific)
[16] Gan C 2006 Noise-induced chaos in Duffing oscillator with double wells *Nonlinear Dyn.* **45** 305–17
[17] Gan C 2006 Pseudo-periodic surrogate test to sample time series in stochastic softening Duffing oscillator *Phys. Lett.* A **357** 204–8
[18] Goggin M E and Milonni P W 1988 Driven Morse oscillator: classical chaos, quantum theory, and photodissociation *Phys. Rev.* A **37** 796–806
[19] Lin Y K and Cai G Q 1995 *Probabilistic Structural Dynamics-Advanced Theory and Applications* (Singapore: McGraw-Hill)
[20] Shinozuka M 1972 Digital simulation of random processes and its applications *J. Sound Vib.* **25** 111–28
[21] Zaslavsky G M 1998 *Physics of Chaos in Hamiltonian Systems* (Oxford: Academic)
[22] Arnold V I 1964 Instability of dynamical systems with several degrees of freedom *Sov. Math. Dokl.* **5** 581–5
[23] Gan C 2006 Noise-induced chaos in a quadratically nonlinear oscillator *Chaos Solitons Fractals* **30** 920–9
[24] Kantz H and Schreiber T 1997 *Nonlinear Time Series Analysis* (Cambridge, UK: Cambridge University Press)
[25] Wolf A, Swift J R, Swinney H L and Vastano J A 1985 Determining Lyapunov exponents from a time series *Physica* D **16** 285–317
[26] Rosenstein M T, Collins J J and Luca C J 1993 A practical method for calculating leading Lyapunov exponents from small data sets *Physica* D **65** 117–34
[27] Takens F 1980 Detecting strange attractors in turbulence *Dynamical Systems and Turbulence, Warwick 1980 (Lecture Notes in Mathematics* vol 898*)* (New York: Springer) pp 366–81
[28] Liebert W and Schuster H G 1989 Proper choice of the time lag for the analysis of chaotic time series *Phys. Lett.* A **142** 107–12
[29] Small M, Xu D and Harrison R G 2001 Surrogate test for pseudo-periodic time series data *Phys. Rev. Lett.* **87** 188101 (1–4)
[30] Small M and Tse C K 2003 Detecting determinism in time series: the method of surrogate data *IEEE Trans. Circuits Syst.* **50** 663–72
[31] Theiler J, Eubank S, Longtin A, Galdrikian B and Farmer J D 1992 Testing for nonlinearity in time series: the method of surrogate data *Physica* **58** 77–94
[32] Judd K 1992 An improved estimator of dimension and some comments on providing confidence intervals *Physica* D **56** 216–28